Tilted waves and passive mode-locking in multi-transverse mode VCSELs

Mathias Marconi, Julien Javaloyes, Stephane Barland, Salvador Balle, Massimo Giudici

Tilted waves and passive mode-locking in multi-transverse mode VCSELs

M. Marconi[1], J. Javaloyes[2], S. Barland[1], S. Balle[2] and M. Giudici[1]
[1] *Institut Non Linaire de Nice, Universit de Nice Sophia Antipolis, Centre National de la Recherche Scientifique, 1361 Route des lucioles, F-06150 Valbonne, France;* [2] *Departament de Fisica, Universitat de les Illes Baleares, C/ Valldemossa, km 7.5, E-07122 Palma de Mallorca, Spain*

We show experimentally that a electrically biased 200 μm multi-transverse mode VCSEL can be passively mode locked using optical feedback from a distant Resonant Saturable Absorber Mirror (RSAM). Optical feedback from RSAM selects a tilted wave propagating along the transverse section of the VCSEL and leading to mode-locking of the external cavity modes. A large portion of the VCSEL transverse section contribute to mode-locked pulse emission leading to pulses of approximately 1 W peak power and 10 ps width.

The laser mode-locking (ML) phenomena is still a subject of intense research. The complex nonlinear dynamics involving the self-organization of many laser modes remains an fascinating problem that was recently linked to out-of-equilibrium phase transitions [1]. From a practical point of view many applications require sources of short pulse like e.g. medicine, metrology and communications [2]. Passive ML (PML) is arguably one of the most elegant method to obtain such pulses. It is achieved by combining two elements, a laser amplifier providing gain and a saturable absorber (SA) acting as a pulse shortening element. The different dynamical properties of the SA and of the gain create a window for amplification only around the pulse [3, 4]. PML can also be achieved using artificial SA like e.g. nonlinear polarization rotation [5], Kerr lens mode locking [6], Crossed-Polarization [7] or Stark effect modulation [8]. The PML mechanism has led to the shortest and most intense optical pulses ever generated and pulses in the femtosecond range are produced by dye [9] and solid state lasers [10]. However, the large size of these devices and the need for optical pumping strongly limit their application domain. More compact solution can be envisaged using semiconductor devices [11?]. Large output power in the Watt range is commonly achieved by coupling vertical external-cavity surface-emitting lasers (VECSEL) with a semiconductor saturable absorber mirror (SESAM). The external cavity is designed to operate in the fundamental Gaussian mode while a large section of the VECSEL is optically pumped to achieve large power. External cavity size leads to repetition rates from few to tens GHz. PML is obtained also in monolithic edge-emitting semiconductor lasers which have the advantage of being electrically biased and to operate at high repetition rate 1 $\sim$ 160 GHz. In both schemes, the presence of higher order transverse modes of the resonator is usually perceived as detrimental for mode-locking stability and it is avoided by cavity designed. On the other hand, the possibility of achieving a cooperative effect of transverses modes for which they would contribute to longitudinal mode locking is very attractive for increasing the pulse power. Moreover, the optical power that can be extracted from a semiconductor laser is limited because of Catastrophic Optical Damage (COD). One path used to circumvent this limit is to increase the volume of the lasing mode, which in the simplest case is achieved by increasing the lateral dimension. However, the emission profile of these lasers usually presents a low quality. This originates from the presence of many lateral modes that are nearly degenerated in gain. This leads to multipeaked near-fields, but more important, the spatial profile usually depends on the current value due to carrier-induced self-focusing, which might even lead to chaotic filamentation of the beam [12]. The origin of this phenomenon is the so-called Spatial Hole Burning (SHB): in regions of high optical intensity, the local gain (and thus the local carrier density) is depressed by stimulated emission; this depression leads to a local increase of refractive index which tends to further confine the light and to increase the local field intensity.

In this work we propose a scheme for achieving mode locking using an electrically biased, 200 μm section VCSEL. This device is mounted in an external cavity configuration closed by a resonant saturable absorber mirror (RSAM). We show that a large section of the device contribute to mode-locking leading to pulses of 10 ps width and around 1 W of peak power.

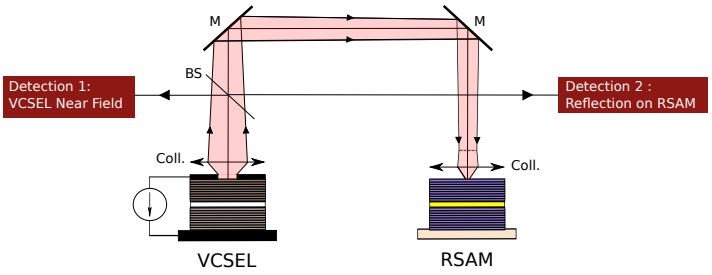

Figure 1: Experimental Set-up: Temperature-stabilized VCSEL and RSAM coopled together. Coll.: Aspheric Lens, BS : Beam Splitter, M: Mirror

The VCSEL is a 980 nm device manufactured by ULM photonics [13]. Its standalone threshold (J_{st}) is about $380mA$, though emission is localized only at the external perimeter of the device up to J=850 mA, after which roll-off starts to occur. At its cavity resonance, which

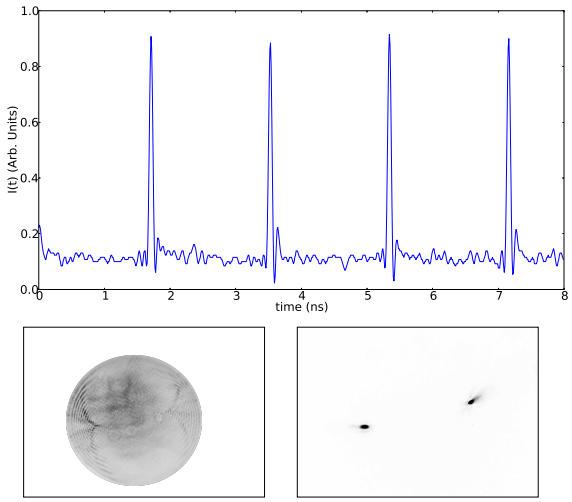

Figure 2: Panel a): Temporal trace of the VCSEL in the mode-locked regime. Panel b): Corresponding Near-Field emission of VCSEL. Panel c): Corresponding Far-field emission from the VCSEL. Intensity grows from white to black. J=600 mA

wavelength can be thermally tuned, the RSAM (BaTop Gmbh) has a low unsaturated reflectivity of 1% that increases to 60% when saturated. The RSAM has an unsaturated cavity resonance with FWHM around 16 nm, a saturation fluence of 15 $\mu J/cm^2$ and a recovery time around 1 ps.

The set up is shown in Fig. 1. Both the VCSEL and RSAM are mounted on temperature controlled substrates which allow for tuning the resonance frequency of each cavity; parameters are set for having the emission of the VCSEL resonant with the RSAM at the VCSEL operating current. The light emitted by the VCSEL is collected by a large numerical aperture (0.68) aspheric lens and the same kind of lens is placed in front of the RSAM. A 10% reflection beam splitter allows for light extraction from the external cavity. The light emitted by the VCSEL is monitored by a 33 GHz scope coupled with fast detectors (8 GHz or 42 GHz). Part of the light is sent to two CCD cameras; the first one records the near-field profile of the VCSEL, while the second records the VCSEL's far-field profile. The light reflected by the RSAM is also used for monitoring and a third CCD camera records the light on the RSAM surface. The external cavity length L is fixed at around 30 cm. One of the most important parameters for achieving mode locking in this setup is the imaging condition of the VCSEL onto the RSAM. We obtain mode-locking when the RSAM is placed in the fourier plane of the VCSEL near-field, a working condition that is obtained by finely tuning the position of the two aspheric lenses placed in front of the VCSEL and of the RSAM. We remark that this leads to a non-local feedback from the RSAM onto the VCSEL: if the RSAM were a normal mirror, the VCSEL near-field profile would be inversely imaged onto itself after a cavity roundtrip.

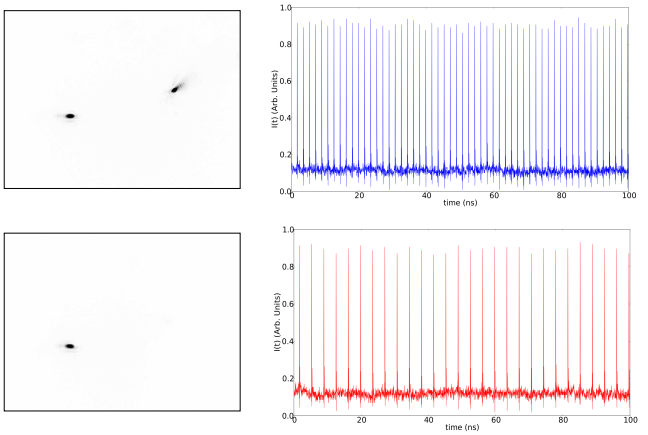

Figure 3: panel a) Time signal obtained when detecting the two spots of the far-field emission of the VCSEL. Panel b) Time signal obtained when detecting a single spot of the far-field emission of the VCSEL

Panel a) in Fig. 2 displays the time trace of the VCSEL in mode-locking regime, that consists of a regular train of pulses with a period equal to the roundtrip time $\tau_e = \frac{c}{2L}$. The pulse width cannot be determined from the oscilloscope traces, which are clearly limited by our real-time detection system (34 GHz bandwidth). An estimate of the pulse width can be obtained from the optical spectrum of the output, which exhibits a broad spectral peak of FWHM around 0.12 nm that corresponds —assuming a linewidth enhancement factor $\alpha \sim 2$ for the VCSELs— to a pulse width around 10 ps FWHM.

Panels b) and c) in Fig.2 show the time-averaged near-field and far-field profiles of the VCSEL, respectively. The image of the RSAM surface is very similar to Fig. 2c), thus revealing that the RSAM is effectively placed in the fourier plane of the VCSEL's near-field. The far-field of the VCSEL exhibits two bright, off-axis spots that indicate the presence of two counter-propagating tilted waves along the cross section of the VCSEL. The transverse wave vector of each of these waves is related in direction and modulus to the position of the spots, and their symmetry with respect to the optical axis indicates that the two transverse wavevectors are one opposite to the other.

Remarkably, however, no interference pattern is visible in the near-field emission. The concentric rings close to the limit of the VCSEL do not contribute significantly to the bright spots in the far-field, as it was verified by filtering out these rings. The lack of interference pattern between the counter-propagating waves in the time-averaged near field implies that the transverse waves must not be simultaneously present, exhibiting anti-phase dynamics. This is apparent in Fig. 3, where the trace from the whole far-field is compared to that from only one of the bright spots. While the emission from the whole far-field has the characteristics discussed above, that emitted by only one of the spots consists also of a periodic train of pulses, but the period is

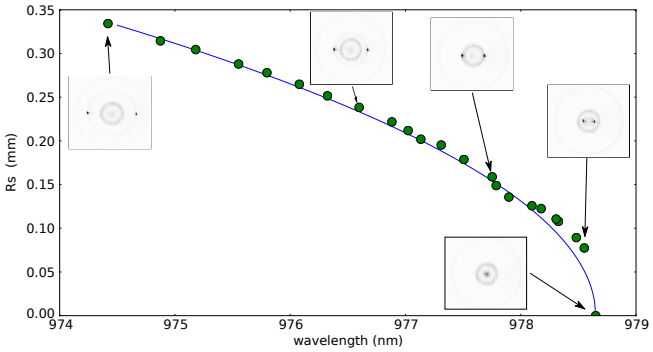

Figure 4: Upper panel: Off axis position of a single spot in the far-field profile as a function of the spectral emission peak of the VCSEL. Far field profile is shown for a number of points in the graph. VCSEL emission is in the mode locking regime for all points of the graph except for the one at the highest wavelength, where a single on axis spot appear in the far-field profile. VCSEL is biased at 700 mA. The transverse wave vector is selected by laterally shifting the lenses in front of the RSAM. The green line has been obtained plotting $r_s = \frac{\lambda_0 f}{2\pi}\sqrt{(\frac{1}{\lambda^2}-\frac{1}{\lambda_0^2})}$, with $\lambda_0 = 978.65nm$ and $f = 8mm$.

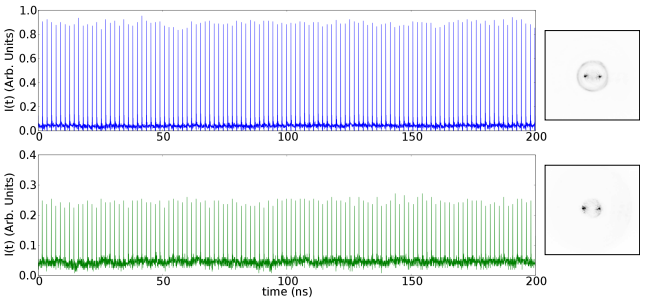

Figure 5: VCSEL time traces emission and corresponding far-field emission profile in the mode-locking regime for two values of the VCSEL bias. Upper panel $J = 703mA$, Lower Panel $J = 285mA$

$2\tau_e$. Thus the trace from the whole far-field is obtained by interleaving two identical pulse trains of period $2\tau_e$ with a delay τ_e of one with respect to the other, each corresponding to a tilted wave with opposite transverse wavevector.

This mode-locked dynamics does not critically depend on the transverse wavevector selected by the system. This can be modified by adjusting the external cavity alignment, namely tilting one of the mirrors M in the set-up or slightly displacing the collimator off the axis defined by the centers of the VCSEL and the RSAM. The change in selected transverse wavevector is evidenced by the variations in the separation between the two spots on the RSAM mirror, as shown in Fig. 4. The position of the spot on the RSAM with respect to the optical axis is related to the transverse wavevector $\vec{K}_\perp = \vec{K} - \vec{K}_0$ of the plane wave by

$$\vec{r}_s = \lambda f \frac{\vec{K}_\perp}{2\pi} \ ,$$

where f is the focal length of the lens in front of the RSAM, λ is the wavelength of the light, $\vec{K}$ is the wavevector emitted by the VCSEL while $\vec{K}_0$ is its component along the cavity axis.

Although substantial changes in emission wavelength —over 4 nm tuning— can be induced in this way, it is observed that within a wide parameter range, the pulse period does not change and the only noticeable effect is a slight reduction of the pulse peak power. We attribute this effect to the increased losses of the external cavity, since the degree of superposition of the VCSEL profile onto its fed back image decreases. Nevertheless, we remark that even for mismatches of the order of the VCSEL radius, the mode-locking dynamics remains. However, when the separation of the spots on the RSAM is exceedingly large, mode-locking is suddenly lost as a result of a too lossy external cavity because of misalignment. More important, mode-locking also disappears suddenly as the two spots are brought to coincide, thus suggesting that plane-wave emission parallel to the optical axis of the VCSEL resonator does not allow for achieving mode-locking. In terms of bias current, the mode-locking regime is stable in a very broad range, namely $285mA < J < 703mA$. When the current is varied in this interval we did not observe any change in the separation between the two bright spots in the far-field profile corresponding to the two tilted waves (4, lower panel). On the other hand the spectral peak corresponding to the mode-locking emission has shifted from 978 nm ($J = 703\ mA$) down to 976 nm ($J = 285mA$), thus showing that the selection of $K_\perp$ does not depend on the detuning between the two cavities at least in the range spanned.

These observations disclose a possible explanation about the emergence of the mode-locking regime in our system. From the dynamical point of view, mode-locking is favored when the saturable absorber is more easily saturated than the amplifier [2]. In our conditions, this can be more easily achieved when the VCSEL emits in the form of a plane wave, which imposes a low power density (hence low saturation) to the gain section and, at the same time, a strong local saturation of the RSAM. This is because in our setup the VCSEL and the RSAM lie on conjugate Fourier planes, hence any plane wave emitted by the VCSEL yields a spot on the RSAM and viceversa. On the other hand, the unsaturated reflectivity of the RSAM is very low ($\sim 1\%$) on resonance, rising up to $\sim 60\%$ when fully saturated. Hence, if the VCSEL emits a pulse in the form of a plane wave with a transverse wavevector $\vec{K}_\perp$, all the power will concentrate on a single spot at $\vec{r}_s$ on the RSAM, hereby strongly saturating the RSAM which becomes reflective. The light thus comes back to the VCSEL, where it arrives with a transverse component $-\vec{K}_\perp$. Upon amplification and reflection at the VCSEL, the process repeats for this plane wave with opposite transverse wavevector, which is now imaged onto the RSAM at $-\vec{r}_s$. Thus, after two

roundtrips the original wave at $\vec{K}_\perp$ overlaps with itself, leading to a pulse train at twice the roundtrip time for this wave which is interleaved with a replica for the opposite wave with a delay of one roundtrip. This explains the observed dynamics, and also the lack of interference pattern in the form of rolls on the VCSEL: even if two tilted waves are then propagating within the VCSEL resonator, they alternate in time with a delay of one roundtrip in the external cavity, so they never coexist and do not yield the expected interference pattern; the two spots in the far-field (i.e., over the RSAM) are only an artifact of time-averaging operated by CCD cameras.

The above scenario holds for any transverse wavevector $\vec{K}_\perp$, and wavevector selectivity arises from several factors. On one hand, both the VCSEL and the RSAM are Fabry-Perot cavities defined by Bragg mirrors which have an angular dependence of their complex reflectivity. Moreover, the reflectivity of a Fabry-Perot cavity depends not only on the wavelength but also on the angle of incidence of the light, and the resonant wavelength of the cavity blue-shifts as the incidence angle increases. This effect is still larger in our system due to the compound-cavity effect. On the other hand, a preferential transverse wavevector can be externally imposed on the beam emitted by the VCSEL by tilting a mirror or —due to the finite size of the VCSEL— by displacing the colimator off axis, and the angle-dependent reflectivities in the external cavity may further enhance this transverse wavevector. Finally, wavevector selectivity may also arise from any imperfections on the RSAM/VCSEL mirrors that break the spatial invariance. The fact that the characteristics of the mode-locked pulse train do not depend on the transverse wavevector selected by the setup opens the very interesting possibility of stirring the mode-locked beam by controlling the position where the spot on the RSAM appears. This could be achieved e.g. optically by injecting an external beam tilted with respect to the optical axis, hereby allowing for optical beam stirring.

In conclusion, we have shown that electrically biased broad-area VCSELs can be passively mode-locked by using feedback from an RSAM when the VCSEL and RSAM are placed on conjugate Fourier planes. The VCSEL then emits a train of pulses of width ~ 10 ps with a period equal to the roundtrip time in the external cavity, τ_e. Inspection of the far-field of the VCSEL reveals two bright peaks symmetrically located around the optical axis which indicate that the VCSEL emits tilted waves, but no interference pattern is visible in the near field. Monitoring the intensity in each of these spots, a pulse train with period $2\tau_e$ and the same pulse width ~ 10 ps is observed. The pulse train from one spot is delayed by one roundtrip with respect to the other, so the two tilted waves never coexist —hence no interference pattern arises— and the total emission from the VCSEL is obtained by interleaving these two pulse trains.

[1] A. Gordon and B. Fischer. Phase transition theory of many-mode ordering and pulse formation in lasers. *Physical Review Letters*, 89:103901–3, 2002.

[2] H. A. Haus. Mode-locking of lasers. *IEEE J. Selected Topics Quantum Electron.*, 6:1173–1185, 2000.

[3] H. A. Haus. Theory of mode locking with a fast saturable absorber. *Journal of Applied Physics*, 46:3049–3058, 1975.

[4] H. A. Haus. Theory of mode locking with a slow saturable absorber. *Quantum Electronics, IEEE Journal of*, 11:736–746, 1975.

[5] H.J.S. Dorren, D. Lenstra, Yong Liu, M.T. Hill, and G.-D. Khoe. Nonlinear polarization rotation in semiconductor optical amplifiers: theory and application to all-optical flip-flop memories. *Quantum Electronics, IEEE Journal of*, 39(1):141–148, Jan 2003.

[6] E. P. Ippen. Principles of passive mode locking. *Appl. Phys. B*, 58:159–170, 1994.

[7] Julien Javaloyes, Josep Mulet, and Salvador Balle. Passive mode locking of lasers by crossed-polarization gain modulation. *Phys. Rev. Lett.*, 97:163902, Oct 2006.

[8] K. G. Wilcox, Z Mihoubi, G. J. Daniell, S. Elsmere, A. Quarterman, I. Farrer, D. A. Ritchie, and A. Tropper. Ultrafast optical stark mode-locked semiconductor laser. *Opt. Lett.*, 33(23):2797–2799, 2008.

[9] R. Fork, C. Shank, R. Yen, and C. Hirlimann. Femtosecond optical pulses. *Quantum Electronics, IEEE Journal of*, 19(4):500 – 506, apr 1983.

[10] U. Keller, K. J. Weingarten, F. X. Kärtner, D. Kopf, B. Braun, I. D. Jung, R. Fluck, C. Hönninger, N. Matuschek, and J. Aus der Au. Semiconductor saturable absorber mirrors (SESAM's) for femtosecond to nanosecond pulse generation in solid-state lasers. *Selected Topics in Quantum Electronics, IEEE Journal of*, 2:435–453, 1996.

[11] E. A. Avrutin, J. H. Marsh, and E. L. Portnoi. Monolithic and multi-GigaHertz mode-locked semiconductor lasers: Constructions, experiments, models and applications. *IEE Proc.-Optoelectron.*, 147:251–278, 2000.

[12] G. H. B. Thompson. A theory for filamentation in semiconductor lasers including the dependence of dielectric constant on injected carrier density. *Opto-electronics*, 4:257–310, 1972.

[13] M. Grabherr, R. Jager, M. Miller, C. Thalmaier, J. Herlein, R. Michalzik, and K.J. Ebeling. Bottom-emitting vcsel's for high-cw optical output power. *Photonics Technology Letters, IEEE*, 10(8):1061–1063, Aug 1998.